

## Improved lead and bismuth ( $n,\gamma$ ) cross sections and their astrophysical impact

C. Domingo-Pardo<sup>1,2,a</sup>, U. Abbondanno<sup>3</sup>, G. Aerts<sup>4</sup>, H. Álvarez<sup>5</sup>, F. Álvarez-Velarde<sup>6</sup>, S. Andriamonje<sup>4</sup>, J. Andrzejewski<sup>7</sup>, P. Assimakopoulos<sup>†8</sup>, L. Audouin<sup>9</sup>, G. Badurek<sup>10</sup>, P. Baumann<sup>11</sup>, F. Bečvář<sup>12</sup>, E. Berthoumieux<sup>4</sup>, F. Calviño<sup>13</sup>, M. Calviani<sup>14,15</sup>, D. Cano-Ott<sup>6</sup>, R. Capote<sup>16,17</sup>, C. Carrapiço<sup>4,18</sup>, P. Cennini<sup>19</sup>, V. Chepel<sup>20</sup>, E. Chiaveri<sup>19</sup>, N. Colonna<sup>21</sup>, G. Cortes<sup>22</sup>, A. Couture<sup>23</sup>, J. Cox<sup>23</sup>, M. Dahlfors<sup>19</sup>, S. David<sup>9</sup>, I. Dillmann<sup>1</sup>, W. Dridi<sup>4</sup>, I. Duran<sup>5</sup>, C. Eleftheriadis<sup>24</sup>, M. Embid-Segura<sup>6</sup>, L. Ferrant<sup>†9</sup>, A. Ferrari<sup>19</sup>, R. Ferreira-Marques<sup>20</sup>, K. Fujii<sup>3</sup>, W. Furman<sup>25</sup>, I. Gonçalves<sup>20</sup>, E. González-Romero<sup>6</sup>, F. Gramegna<sup>14</sup>, C. Guerrero<sup>6</sup>, F. Gunsing<sup>4</sup>, B. Haas<sup>26</sup>, R. Haight<sup>27</sup>, M. Heil<sup>1</sup>, A. Herrera-Martinez<sup>19</sup>, M. Igashira<sup>28</sup>, E. Jericha<sup>10</sup>, F. Käppeler<sup>1</sup>, Y. Kadi<sup>19</sup>, D. Karadimos<sup>8</sup>, D. Karamanis<sup>8</sup>, M. Kerveno<sup>11</sup>, P. Koehler<sup>29</sup>, E. Kossionides<sup>30</sup>, M. Krťička<sup>12</sup>, C. Lampoudis<sup>4,24</sup>, H. Leeb<sup>10</sup>, A. Lindote<sup>20</sup>, I. Lopes<sup>20</sup>, M. Lozano<sup>17</sup>, S. Lukic<sup>11</sup>, J. Marganiec<sup>7</sup>, S. Marrone<sup>21</sup>, T. Martínez<sup>6</sup>, C. Massimi<sup>31</sup>, P. Mastinu<sup>14</sup>, A. Mengoni<sup>16,19</sup>, P.M. Milazzo<sup>3</sup>, C. Moreau<sup>3</sup>, M. Mosconi<sup>1</sup>, F. Neves<sup>20</sup>, H. Oberhummer<sup>10</sup>, S. O'Brien<sup>23</sup>, J. Pancin<sup>4</sup>, C. Papachristodoulou<sup>8</sup>, C. Papadopoulos<sup>32</sup>, C. Paradela<sup>5</sup>, N. Patronis<sup>8</sup>, A. Pavlik<sup>33</sup>, P. Pavlopoulos<sup>34</sup>, L. Perrot<sup>4</sup>, M.T. Pigni<sup>10</sup>, R. Plag<sup>1</sup>, A. Plompen<sup>35</sup>, A. Plukis<sup>4</sup>, A. Poch<sup>22</sup>, J. Praena<sup>14</sup>, C. Pretel<sup>22</sup>, J. Quesada<sup>17</sup>, T. Rauscher<sup>36</sup>, R. Reifarth<sup>27</sup>, C. Rubbia<sup>37</sup>, G. Rudolf<sup>11</sup>, P. Rullhusen<sup>35</sup>, J. Salgado<sup>18</sup>, C. Santos<sup>18</sup>, L. Sarchiapone<sup>19</sup>, I. Savvidis<sup>24</sup>, C. Stephan<sup>9</sup>, G. Tagliente<sup>21</sup>, J.L. Tain<sup>2</sup>, L. Tassan-Got<sup>9</sup>, L. Tavora<sup>18</sup>, R. Terlizzi<sup>21</sup>, G. Vannini<sup>31</sup>, P. Vaz<sup>18</sup>, A. Ventura<sup>38</sup>, D. Villamarin<sup>6</sup>, M.C. Vicente<sup>6</sup>, V. Vlachoudis<sup>19</sup>, R. Vlastou<sup>32</sup>, F. Voss<sup>1</sup>, S. Walter<sup>1</sup>, M. Wiescher<sup>23</sup>, and K. Wisshak<sup>1</sup>

The n\_TOF Collaboration (www.cern.ch/ntof)

<sup>1</sup>Forschungszentrum Karlsruhe GmbH (FZK), Institut für Kernphysik, Germany – <sup>2</sup>Instituto de Física Corpuscular, CSIC-Universidad de Valencia, Spain – <sup>3</sup>Istituto Nazionale di Fisica Nucleare, Trieste, Italy – <sup>4</sup>CEA/Saclay-DSM/DAPNIA, Gif-sur-Yvette, France – <sup>5</sup>Universidad de Santiago de Compostela, Spain – <sup>6</sup>Centro de Investigaciones Energeticas Medioambientales y Tecnológicas, Madrid, Spain – <sup>7</sup>University of Lodz, Lodz, Poland – <sup>8</sup>University of Ioannina, Greece – <sup>9</sup>Centre National de la Recherche Scientifique/IN2P3-IPN, Orsay, France – <sup>10</sup>Atominstytut der Österreichischen Universitäten, Technische Universität Wien, Austria – <sup>11</sup>Centre National de la Recherche Scientifique/IN2P3-IREs, Strasbourg, France – <sup>12</sup>Charles University, Prague, Czech Republic – <sup>13</sup>Universidad Politécnica de Madrid, Spain – <sup>14</sup>Istituto Nazionale di Fisica Nucleare, Laboratori Nazionali di Legnaro, Italy – <sup>15</sup>Dipartimento di Fisica, Università di Padova, Italy – <sup>16</sup>International Atomic Energy Agency (IAEA), Nuclear Data Section, Vienna, Austria – <sup>17</sup>Universidad de Sevilla, Spain – <sup>18</sup>Instituto Tecnológico e Nuclear (ITN), Lisbon, Portugal – <sup>19</sup>CERN, Geneva, Switzerland – <sup>20</sup>LIP-Coimbra & Departamento de Física da Universidade de Coimbra, Portugal – <sup>21</sup>Istituto Nazionale di Fisica Nucleare, Bari, Italy – <sup>22</sup>Universitat Politècnica de Catalunya, Barcelona, Spain – <sup>23</sup>University of Notre Dame, Notre Dame, USA – <sup>24</sup>Aristotle University of Thessaloniki, Greece – <sup>25</sup>Joint Institute for Nuclear Research, Frank Laboratory of Neutron Physics, Dubna, Russia – <sup>26</sup>Centre National de la Recherche Scientifique/IN2P3 - CENBG, Bordeaux, France – <sup>27</sup>Los Alamos National Laboratory, New Mexico, USA – <sup>28</sup>Tokyo Institute of Technology, Tokyo, Japan – <sup>29</sup>Oak Ridge National Laboratory, Physics Division, Oak Ridge, USA – <sup>30</sup>NCSR, Athens, Greece – <sup>31</sup>Dipartimento di Fisica, Università di Bologna, and Sezione INFN di Bologna, Italy – <sup>32</sup>National Technical University of Athens, Greece – <sup>33</sup>Institut für Isotopenforschung und Kernphysik, Universität Wien, Austria – <sup>34</sup>Pôle Universitaire Léonard de Vinci, Paris-La Défense, France – <sup>35</sup>CEC-JRC-IRMM, Geel, Belgium – <sup>36</sup>Department of Physics, University of Basel, Switzerland – <sup>37</sup>Università degli Studi Pavia, Pavia, Italy – <sup>38</sup>ENEA, Bologna, Italy

**Abstract.** A series of ( $n,\gamma$ ) neutron capture measurements on the lead isotopes and bismuth have been carried out at the CERN n\_TOF installation in the neutron energy range from 1 eV up to 1 MeV. At n\_TOF, contaminations due to scattered neutrons were reduced down to a negligible level by using improved  $\gamma$ -ray detectors with very low neutron sensitivity. The background level has been determined precisely from a complementary measurement. Other experimental effects related to the electronic threshold in the detectors and the angular distribution of the prompt  $\gamma$ -rays were investigated via Monte Carlo simulations and could be taken in account in the analysis of the capture data. With this set of measurements the energy differential ( $n,\gamma$ ) cross sections of <sup>204,206,207</sup>Pb and <sup>209</sup>Bi have been determined with good accuracy. The information obtained in this work becomes of interest for constraining  $r$ -process calculations and in particular for the Th/U cosmochronometer.

### 1 Introduction

The heavy elements lead and bismuth are synthesized by both the slow ( $s$ -) and the rapid ( $r$ -) neutron capture processes. In this mass region the  $s$ -process takes place in the framework of

a complicated network (see fig. 1), where the abundances are affected by several branching points (<sup>204</sup>Tl, <sup>210</sup>Bi and <sup>210</sup>Po). Due to this complex scenario the  $s$ -process abundances of these isotopes are sensitive to the different neutron irradiation periods during the evolution of the Asymptotic Giant Branch (AGB) stage of stellar evolution, where these isotopes are produced [1–4].

<sup>a</sup> Presenting author, e-mail: cesar.domingo.pardo@cern.ch

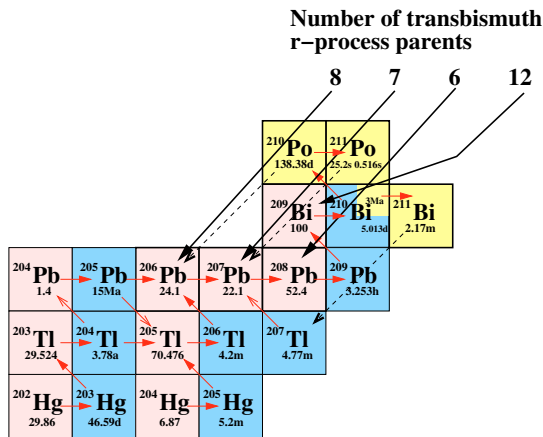


**Fig. 1.** Nucleosynthesis path of the *s*-process in the Pb-Bi region. The number of short lived transbismuth isotopes contributing to the *r*-process nucleosynthesis of these elements is shown with solid black arrows.

On the other hand, the *r*-process contribution to these isotopes is strongly dominated (90%) by the decay of the short lived transbismuth isotopes [5]. For this reason, the *r*-process fraction  $N_r$ , derived from the rather reliably known total abundance in the solar system  $N_{\odot}$ ; and from the *s*-process  $N_s$  component,

$$N_r = N_{\odot} - N_s, \quad (1)$$

constitutes an important constraint for *r*-process model calculations. This aspect is also important for the age estimates based on observed actinide abundances in ultra metal poor stars.

Because the cross sections of these isotopes are dominated by resonances where neutron scattering is large compared to the  $(n,\gamma)$  channel, their capture cross sections can be best measured by using small volume (total energy) detectors, which can be optimized in order to reduce backgrounds due to scattered neutrons. This method requires the use of the so-called Pulse Height Weighting Technique (PHWT) [6], which makes the capture detection probability independent of the particular decay path. This technique is based on the precise knowledge of the detector response to capture  $\gamma$ -rays. Weighting Functions (WFs) obtained in the early days when the technique was proposed, resulted in accuracies not better than 20% in some particular cases [7]. A combined analysis of measurements made at Geel [8] and Monte Carlo (MC) simulations and measurements made at ORNL [9] for the particular case of <sup>56</sup>Fe revealed that the problem was due to incorrect WFs used in the analysis of previous measurements. The issue of an inaccurate WF concerns also measurements made 20–30 years ago on <sup>204</sup>Pb [10,11], <sup>206</sup>Pb [10,12], <sup>207</sup>Pb [10,13,14] and Bi [15], but also more recent measurements [16] on <sup>207</sup>Pb and Bi, which were analyzed with a single experimentally determined WF in a sandwiched sample set-up for an improved accuracy [8]. With today's MC codes one can obtain realistic detector responses using precise modellizations of experimental setups [17–20], which allows in combination with an accurate method [18,19] to obtain reliable WFs.

The effect of an incorrect WF on the capture yield is difficult to quantify accurately. It might be small for isotopes

or resonances with capture  $\gamma$ -ray spectra similar to the resonance used as reference for absolute yield normalization (like the 4.9 eV resonance in gold), or it might be as large as 16% for resonances with a “harder” spectrum [21]. The fact that many resonances in the lead isotopes show a very hard pulse height spectrum (dominated by only one or two step cascades) motivated a new measurement of these isotopes using improved weighting functions.

The hard pulse height spectra in some of these isotopes, mainly <sup>206</sup>Pb, has the additional experimental difficulty that the prompt  $\gamma$ -rays for certain resonances with  $l > 0$  show an anisotropic angular distribution. This effect can be also minimized by utilizing a setup where the detectors are placed at 125° with respect to the incident neutron beam direction. Additionally some other experimental aspects could be also improved. Previous capture measurements of <sup>204</sup>Pb were made in the neutron energy range above 2.5 keV, which hindered the measurement of a few resonances below that energy. Finally the neutron sensitivity of the capture setup has been extremely improved (see refs. [22,23]) when compared to the original setups based on C<sub>6</sub>F<sub>6</sub> detectors surrounded by rather massive structural materials.

## 2 The CERN n\_TOF facility and experimental setup

The capture cross sections of <sup>204,206,207</sup>Pb and Bi were measured as a function of the energy via the time of flight technique at the CERN n\_TOF installation [24]. At n\_TOF neutrons are produced by a 20 GeV proton beam on a lead spallation target. The beam is characterized by intense proton bunches of  $3\text{--}7 \times 10^{12}$  protons, a width of 6 ns rms, and a very low repetition frequency of 0.4 Hz. Thanks to this very low duty cycle, a broad energy range from several MeV down to 1 eV can be measured in each run with favorable background conditions and without having overlapping neutrons from previous runs.

Capture events are registered with two small (1 l volume) C<sub>6</sub>D<sub>6</sub> scintillators. The detectors [23] and the experimental setup [24,25] were optimized in order to minimize backgrounds from sample-scattered neutrons.

Because of the importance of accurate WFs (see sect. 1), much effort has been put at n\_TOF in order to use the PHWT properly. Therefore the 1.15 keV resonance on <sup>56</sup>Fe, which has been found to be particularly sensitive to the shape of the calculated WF [9], was measured with two different types of C<sub>6</sub>D<sub>6</sub> detectors and with iron samples of three different thicknesses (from 0.5 mm to 2 mm). By this study it was verified that an uncertainty better than 2% can be achieved with WFs derived from MC simulations [19]. This result is in excellent agreement with the pioneering work of Perey et al. [9], who found an uncertainty of 3% for a sample 0.5 mm in thickness with WFs obtained from response functions, which were simulated with the MC code EGS4 [26]. The accuracy shown by the MC calculations in the latter two studies is considerably better than the results obtained by Gayther et al. [27], who found an uncertainty of ~6% for a 0.3 mm thick Fe sample and 11% for a thicker (2 mm) iron sample, also employing EGS4 for simulating the responses. This illustrates the need to confront the effect of the MC calculated WFs

with sensitive measurements (like the 1.15 keV resonance in  $^{56}\text{Fe}$ ), in order to have a realistic estimate of the quality of the simulation and the related uncertainties.

The measurement of the lead isotopes at n\_TOF was made with the two  $\text{C}_6\text{D}_6$  detectors placed at an angle of about  $125^\circ$  degrees with respect to the incident neutron beam direction in order to minimize angular distribution effects of the prompt capture  $\gamma$ -rays.

The dependence of the neutron flux versus neutron energy was determined with an accuracy of  $\pm 2\%$  by means of a fission chamber calibrated by the Physikalisch-Technische Bundesanstalt (PTB) [28]. The latter was used to measure the fission yields of  $^{235,238}\text{U}$  samples. During the capture measurements the neutron intensity was also monitored via four silicon detectors, which registered the  $^3\text{H}$  and  $\alpha$  particles from a thin  $^6\text{Li}$  foil centered in the beam [25].

### 3 Capture data analysis

The WFs required for the analysis of each isotope and for the gold reference sample were determined from a set of  $\gamma$ -rays response functions obtained from a GEANT4 Monte Carlo simulation, where the experimental setup and the particular capture sample were carefully modeled. A realistic 3-dimensional generation of events inside the cylindrical samples was implemented in the simulation code. In the radial direction of the sample  $\gamma$ -rays were generated with the n\_TOF beam profile distribution [29]. Across the sample thickness ( $z$ ) a  $\gamma$ -ray emission probability distribution ( $e^{-n\sigma z}$ ) was taken into account. It was found that the large  $\gamma$ -ray absorption effects inside the low cross section and high  $Z$  samples (Pb and Bi) prevent a polynomial WF to appropriately fulfill the proportionality condition between  $\gamma$ -ray energy and efficiency, on which the PHWT is based. We were able to overcome this problem by using a numerical-pointwise WF derived from a very large set of MC simulated response functions to which a linear regularization method was applied [30,31].

The uncertainty introduced in the capture yield due to the WFs calculated for the gold, lead and bismuth sample was estimated on the basis of MC simulations of the complete capture  $\gamma$ -ray spectra [19]. The calculated WFs were applied to the simulated capture spectra and the resulting weighted sum was shown to deviate only  $\sim 0.5\%$  from the corresponding capture energy. This indicates that an error of less than 1% is introduced in the capture yield by the calculated WFs.

For each measured isotope, as well as for the gold reference sample, a resonance (spin-parity dependent) yield correction factor was calculated, which accounts for the fraction of the spectrum missing below the noise-rejecting threshold in the  $\text{C}_6\text{D}_6$  detectors. A  $\text{C}_6\text{D}_6$  threshold between 200 and 300 keV led to yield corrections between 3% and 7%. Other systematic effects related with  $\gamma$ -ray summing in the detectors and conversion electron processes, were also treated within the simulation of the prompt  $\gamma$ -rays cascades and are included in the yield correction factor.

The capture yield was normalized via the saturated resonance technique [32] by measuring a gold sample in regular intervals.

The background for the Pb and Bi isotopes in the entire energy range is dominated by in-beam  $\gamma$ -rays scattered in the

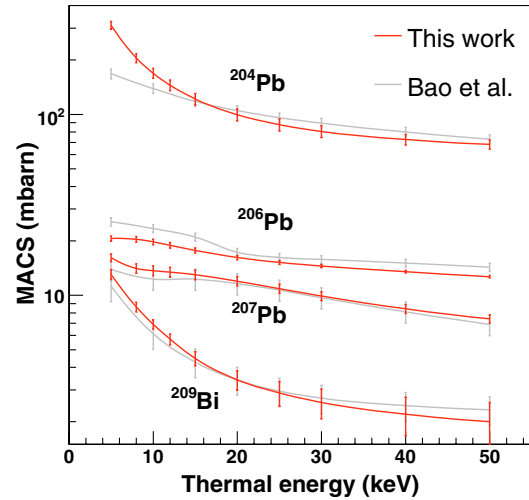


**Fig. 2.** Present MACS determined here for Pb and Bi, compared with the compilation of Bao et al. [34].

capture sample. The dependence of this background with neutron energy was best determined from the measurement of an enriched  $^{208}\text{Pb}$  sample, which showed only a few resonances in the entire energy range.

Finally an  $R$ -matrix analysis of the capture yield was performed using the SAMMY code [33]. Capture areas and resonance parameters ( $E_\sigma$ ,  $\Gamma_\gamma$  and/or  $\Gamma_n$ ) were derived from the fit of the experimental data. In the fitting procedure the background level at each channel (or neutron energy) was fixed rather than subtracted.

### 4 Results and astrophysical implications

A detailed comparison versus previous measurements is out of the scope of this paper. Therefore only the Maxwellian Averaged Cross Sections (MACS) will be compared versus the compilation of Bao et al. [34] (see fig. 2), which has been commonly used so far for stellar  $s$ -process calculations.

The new MACS of  $^{204}\text{Pb}$  at  $kT = 5 - 8$  keV is about 30% larger than reported before. This discrepancy is due to three resonances below 2.6 keV, which were not measured before in capture and apparently were not included in the compilation either. The discrepancy in the case of  $^{206}\text{Pb}$  is more difficult to identify, since they could originate from angular distribution effects of the prompt capture  $\gamma$ -rays or from the WF used in previous measurements [10,12]. Our MACS for  $^{206}\text{Pb}$  is in good agreement with a recent measurement at Geel [35]. For the rest of the isotopes and/or energy regions, the new results show good agreement with the compiled cross sections, which means that the respective uncertainties were properly evaluated. For all isotopes, including  $^{207}\text{Pb}$  and  $^{209}\text{Bi}$ , the uncertainties in the relevant energy regions around 30 keV and 8 keV, have been substantially improved. Consequently, this led to a more accurate determination of the  $s$ -process abundances for these isotopes (see fig. 3).

According to the Galactic chemical evolution (GCE) model [3,4] most of the  $s$ -process abundance of  $^{208}\text{Pb}$  and  $^{209}\text{Bi}$  is synthesized in Asymptotic Giant Branch (AGB) stars of low metallicity. About 95% of the neutron irradiation is

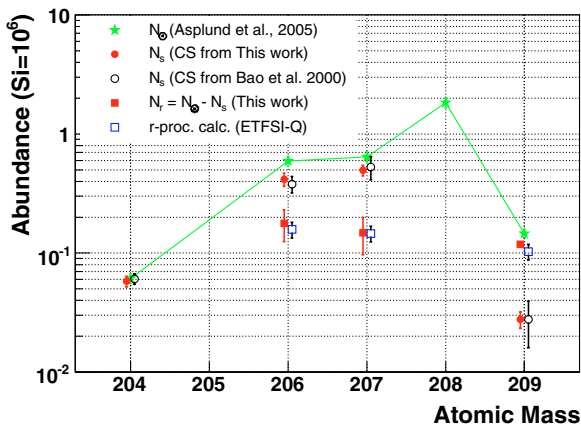


**Fig. 3.** The  $s$ -process abundances (solid circles) derived from the new MACS (fig. 2) are compared to the data obtained with the previous MACS from ref. [34] (open circles). The corresponding solar system abundances [36] are indicated by stars. The  $r$ -process residuals (solid squares) are compared to  $r$ -process model calculations (open squares) taken from the literature [5].

caused by the  $^{13}\text{C}(\alpha, n)^{16}\text{O}$  reaction, which operates during the interpulse phase, at temperatures of  $\sim 10^8$  K or thermal energies of  $kT \approx 8$  keV. In these cases the final abundances are strongly determined by the cross section at 5–10 keV. The abundances were determined for a thermally pulsing AGB star with  $M = 3M_{\odot}$  and a metallicity  $[\text{Fe}/\text{H}] = -1.3$ , characteristic of the strong  $s$ -process component. On the other hand the abundances of  $^{204,206,207}\text{Pb}$  were calculated using a combination of masses  $M = 3M_{\odot}$  and  $M = 1.5M_{\odot}$ , and metallicities  $[\text{Fe}/\text{H}] = -0.3$  and  $[\text{Fe}/\text{H}] = -1.3$ , which account for the main and the strong  $s$ -process components, respectively.

These results are summarized in figure 3, which shows also the same calculation based on the MACS from the compilation. In particular the  $s$ -process abundances of  $^{207}\text{Pb}$  and  $^{209}\text{Bi}$  could be now determined more accurately. Since the  $s$ -process fraction of bismuth relatively small, the  $r$ -process residual becomes a very accurate constraint for  $r$ -process model calculations of the transbismuth region [5, 37, 38].

This work has been partially supported by the EC (contract FIKW-CT-200000107) and by the National Institutions partners in the n\_TOF Collaboration.

## References

1. R. Gallino et al., *Astrophys. J.* **497**, 388 (1998).
2. C. Arlandini et al., *Astrophys. J.* **525**, 886 (1999).

3. C. Travaglio et al., *Astrophys. J.* **521**, 691 (1999).
4. C. Travaglio et al., *Astrophys. J.* **549**, 346 (2001).
5. J.J. Cowan et al., *Astrophys. J.* **521**, 194 (1999).
6. R.L. Macklin, J.H. Gibbons, *Phys. Rev.* **159**, 1007 (1967).
7. R. Macklin, *Nucl. Sci. Eng.* **95**, 200 (1987).
8. F. Corvi et al., *Nucl. Instrum. Meth. Phys. Res. A* **265**, 475 (1988).
9. F.G. Perey et al., in *Nuclear Data for Science and Technology* (Mito, 1988), p. 379.
10. B.J. Allen et al., *Phys. Rev. C* **8**, 1504 (1973).
11. D.J. Horen et al., *Phys. Rev. C* **29**, 2126 (1984).
12. M. Mizumoto et al., *Phys. Rev. C* **19**, 335 (1979).
13. S. Raman et al., *Phys. Rev. Lett.* **39**, 598 (1977).
14. S. Raman et al., *Phys. Rev. Lett.* **40**, 1306 (1978).
15. R. Macklin et al., *Phys. Rev. C* **14**, 1389 (1976).
16. P. Mutti et al., in *Nuclei in the Cosmos*, edited by N. Prantzos, S. Harissopulos (Éditions Frontières, 1998), pp. 204–207.
17. P.E. Koehler et al., *Phys. Rev. C* **54**, 1463 (1996).
18. J.L. Tain et al., in *J. Nucl. Sci. and Technol.* (Tsukuba, 2002), Vol. 2, p. 689.
19. U. Abbondanno et al., *Nucl. Instrum. Meth. Phys. Res. A* **521**, 454 (2004).
20. A. Borella et al., in *International Conference on Nuclear Data for Science and Technology*, AIP Conference Series **769** (2005), pp. 652–655.
21. C.M. Perey et al., *Phys. Rev. C* **47**, 1143 (1993).
22. P.E. Koehler et al., *Phys. Rev. C* **62**, 055803 (2000).
23. R. Plag et al., *Nucl. Instrum. Meth. Phys. Res. A* **496**, 425 (2003).
24. U. Abbondanno et al., *Tech. Rep. CERN-SL-2002-053 ECT* (2003).
25. S. Marrone et al., *Nucl. Instrum. Meth. Phys. Res. A* **517**, 389 (2004).
26. W. Nelson et al., *Tech. Rep. SLAC-265*, Stanford Linear Accelerator Center, 1985 (unpublished).
27. D.B. Gayther et al., in *Nuclear Data for Science and Technology* (Mito, 1988), p. 379.
28. C. Borcea et al., *Nucl. Instrum. Meth. Phys. Res. A* **513**, 524 (2003).
29. J. Pancin et al., *Nucl. Instrum. Meth. Phys. Res. A* **524**, 102 (2004).
30. C. Domingo-Pardo, Ph.D. thesis, CSIC-University of Valencia, 2005.
31. C. Domingo-Pardo et al., *Phys. Rev. C* **74**, 025807 (2006).
32. R. Macklin et al., *Nucl. Instrum. Meth. Phys. Res. A* **164**, 213 (1979).
33. N.M. Larson (2006), SAMMY, computer code Report ORNL/TM-9179/R7, Oak Ridge National Laboratory.
34. Z.Y. Bao et al., *At. Data Nucl. Data Tables* **76**, 70 (2000).
35. A. Borella, Ph.D. thesis, University of Gent, 2005.
36. M. Asplund et al., in *ASP Conf. Ser. 336*, edited by T.G. Barnes, III, F.N. Bash (2005), p. 25.
37. H. Schatz et al., *Astrophys. J.* **579**, 626 (2002).
38. K.-L. Kratz et al., *New Astronomy Review* **48**, 105 (2004).